

LARGE-STRAIN, PIEZOELECTRIC, IN-PLANE MICRO-ACTUATOR

Nicholas J. Conway and Sang-Gook Kim.

Micro and Nano Systems Laboratory, Department of Mechanical Engineering
Massachusetts Institute of Technology, Cambridge Massachusetts, USA

ABSTRACT

A new type of high-force, large displacement, low-voltage piezoelectric actuator has been developed using a compact stroke amplifying mechanism. The device is fabricated using an SU-8 structure as an amplifying mechanism for thin-film PZT. Each actuator “cell” can be arrayed in series and/or in parallel and the design can accommodate different force/displacement requirements. Peak static force of the design tested was 55 μN , and peak static displacement was 1.18 μm at 10V. Fabricated devices consisting of three actuators in series were tested, which showed a strain amplification ratio in excess of 10:1 per cell.

1. INTRODUCTION

Microsystems have relied heavily on electrostatic actuators due to their ease of design and fabrication. In general, electrostatic actuation is adequate for the low force and energy density requirements of many MEMS applications today. Emerging MEMS applications, however, such as MEMS relays, require higher energy density microactuators than the popular electrostatic microactuators. Thin-film piezoelectrics have been known for their high force potential and energy density, compactness, fast dynamic response time, low input power and low driving voltage. The small strain of piezoelectrics (on the order of $\sim 0.1\%$), however, has limited their wide use in many MEMS applications.

To overcome these strain limitations, many stroke amplifying mechanisms have been reported in macro-scale applications [1]. Until recently, few strain amplifying microactuators have been reported. Internally leveraged amplifiers such as bimorph cantilevers have been the popular design of thin-film piezoelectric actuators [2,3], and while they can amplify strain effectively, they suffer from low stiffness, low actuation force, and often only operate out-of-plane. Piezoelectric micro-hydraulic actuators [4] can deliver high force or large stroke selectively, but suffer from bulkiness, possible fluid leakage and slow response. Here we demonstrate a compact, externally-leveraged MEMS device that can amplify piezoelectric stroke in excess of 10 times. With a device cell size of roughly $520 \times 650 \mu\text{m}^2$, the actuator is arrayable in series and/or parallel for additive displacement, force and rigidity in-plane.

2. DESIGN

Figure 1 shows a model of a unit cell actuator and Figure 2 shows an SEM picture of a three-cell series piezoelectric micro-actuator. In each cell, a piezoelectric member made of sol-gel PZT spans the middle of a compliant amplifier made of SU-8. The compliant structure consists of flexural pivots that minimize the energy loss during actuation and four-bar guiding linkages that robustly maintain the direction of the actuation. Actuators in series are powered by a bus (depicted in Figure 2) that runs along the linkage, and has a “loop” appearance.

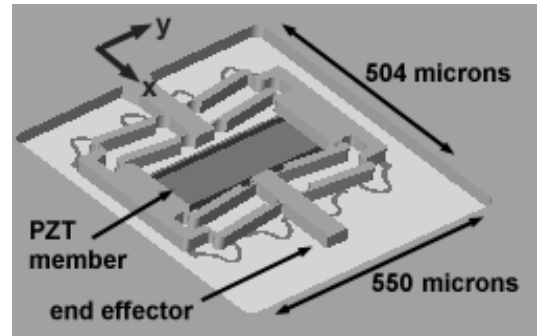


Figure 1: Single-cell amplifying actuator model

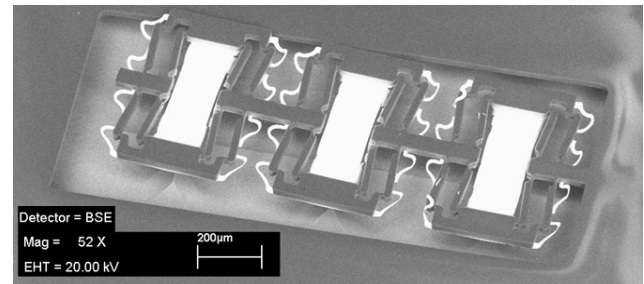


Figure 2: SEM of three-cell amplifying actuator.

The amplification principle depicted in Figure 3 was adopted for the design. Two ends of a link are constrained to move along two perpendicular walls. The angle, θ , that the beam makes with the horizontal wall fully defines the link’s position in space. Let the left end of the link be the input and the right end be the output, defined by x and y respectively. If θ changes from an initial angle, θ_0 , then the change in y versus the change in x is going to be,

$$\frac{\Delta y}{\Delta x} = \frac{\sin \theta - \sin \theta_0}{\cos \theta - \cos \theta_0} = -\cot \frac{1}{2}(\theta + \theta_0), \quad (1)$$

which is plotted in Figure 4. Designing the actuator with a smaller θ_0 will result in larger displacements, this comes at a

trade off in less blocking force. For this work, we chose a $\theta_0 = 5^\circ$ such that acceptable displacement and blocking force could be achieved.

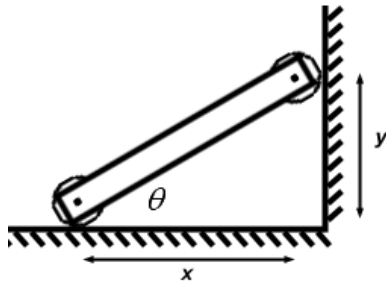


Figure 3: Amplification principle

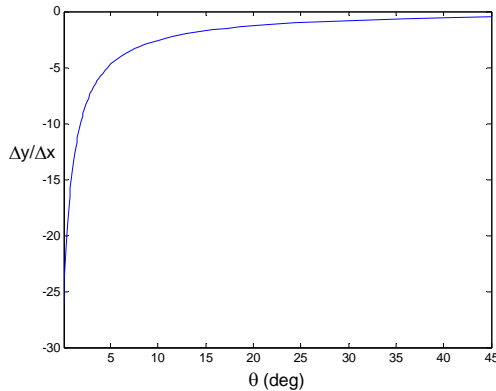


Figure 4: Plot of amplification ratio versus angle and for $\theta_0 = 1^\circ$.

3. FABRICATION

Recent advancements in MEMS have demonstrated that SU-8 can be used for the development of in-plane compliant mechanisms[5]. Since SU-8 requires no etching obtain high-aspect-ratio structures as well as demonstrates excellent mechanical properties[6], it is highly desirable to use in a prototype design. Figures 5 a) through 5 e) show the process flow for device fabrication depicting the cross-sectional structure and fabrication steps of the device

In step a), 2000\AA of SiO_2 is grown by thermal oxidation of a silicon substrate. In step b), lift-off of e-beam evaporated Ti/Pt ($200\text{\AA}/2000\text{\AA}$) is achieved in acetone. The bottom electrode, electrode bus, and alignment marks are formed in this step. In step c), Mitsubishi Materials Co. sol gel PZT (F2) is spin coated, dried (pyrolysis), etched, and then annealed to a thickness of 4000\AA . For simplicity, good perovskite crystal structure is ensured by etching the PZT prior to annealing. Step d) is the same as step two, forming the over lapping (top) electrode of the PZT member. A 30\mu m deposition of SU-8 occurs in step e). The device is dry released by an RIE etch of SiO_2 with CF_4 followed by an isotropic XeF_2 etch to remove underlying silicon. The oxide left under the PZT member shifts the neutral axis and will inevitably cause bending of the PZT member. The oxide is left to maintain fabrication simplicity.

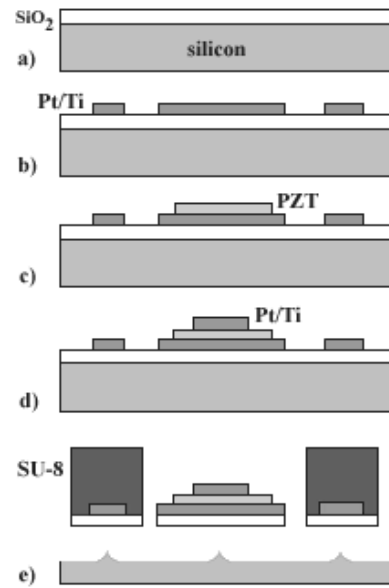


Figure 5: Fabrication process

4. ANALYSIS AND TESTING

In order to ensure that the devices work, a verification of the PZT's polarization was performed prior to actuation measurements. The devices were tested using a probe station to determine the unloaded displacement of the device, and the hysteresis curve of the piezoelectric. The hysteresis curve was measured using an RT66A standardized ferroelectric test system from Radiant Technologies, Inc. of Albuquerque, New Mexico, USA., connected to a PC running Radiant Technologies CHARGE program.

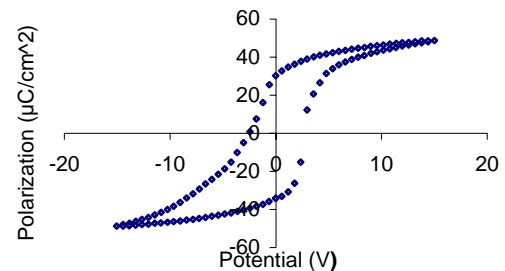


Figure 6: PZT hysteresis of a 0.4\mu m thick film at $15V$

The result in Figure 6 compares favorably with literature [7] with a maximum polarization of $\sim 50\text{\mu C/cm}^2$ for a 0.4\mu m thick film at $15V$ with an area of $11.4 \times 10^{-4}\text{ cm}^2$. The leakage current is $2.58 \times 10^{-6}\text{ A}$ at a resistivity of $1.65 \times 10^8\text{ Ohm-cm}$, both of which are within acceptable tolerances. Care during fabrication is needed to ensure low leakage. Figure 7 shows strong perovskite phases in the XRD. Only perovskite PZT

phases peaks are visible, other than a strong platinum peak. The pyrochlore phase, visible around 29° and 34° if present, is not detectable within the instrument resolution

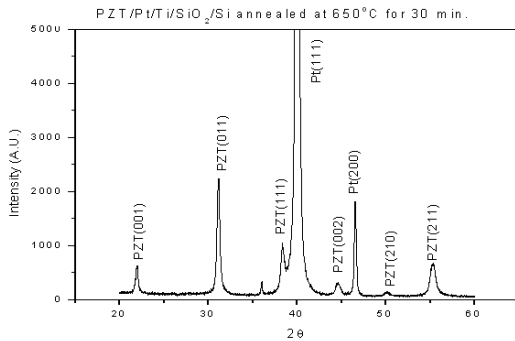


Figure 7: X-Ray diffraction crystallography of the PZT

Measurements of the microactuator (three in series) were performed using the computer microvision system [8]. To determine the low frequency behavior, the microactuator was electrically stimulated with a sinusoidal waveform (DC offset with 1Vp-p, 3Vp-p and 5Vp-p AC) at 100 Hz. Brightfield images were obtained at 8 equally spaced phases of this sinusoidal stimulus waveform. Displacements between the consecutive brightfield images were determined using a gradient method described elsewhere [9]. Displacements in the x-direction are approximately sinusoidal and are plotted as time waveforms for two cycles of the stimulus in Figure 8. The results show a linear increase in peak displacement for a given stimuli which is expected due to the small change in the angle of the links in the amplifying structure and the small range of motion the PZT itself.

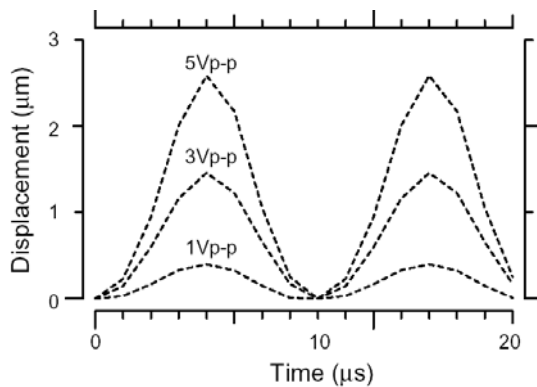


Figure 8: x-displacement (see axis in Fig. 1) of three-cell series driven at 100Hz.

A static force/displacement characterization was developed by measuring free displacement and blocked displacement of the actuator. Figure 9 shows the response of displacement versus applied voltage and Figure 10 shows the developed force displacement characterization, with a

maximum blocked force of 55 μN and free displacement of 1.18 μm at 10 V. The blocked displacement measurement was made with a separate actuator fabricated with a cantilever beam connected to the end effector. Knowing the characteristics of SU-8 very well [6], it is possible to calculate the stiffness of the cantilever beam accurately, and therefore the applied force for a given displacement. In this way, the stiffness of the actuator can be calculated and the blocked force estimated. At static potentials, device operation becomes mildly nonlinear at lower voltages. While bending of the PZT member does cause parasitic losses, the end effector has negligible out of plane motion.

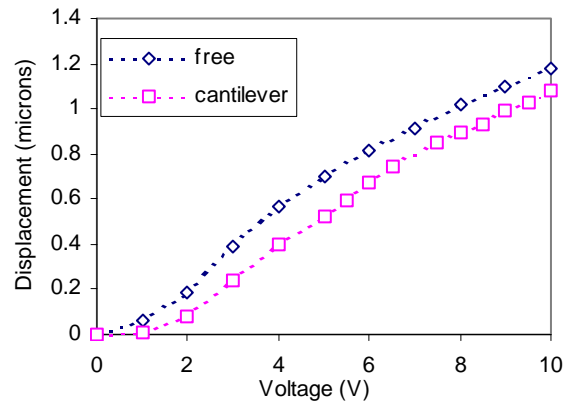


Figure 9: Static end effector x-displacement measurements (see axis in Fig. 1) determined using the computer microvision system adapted for static measurements. Three-cell series measured.

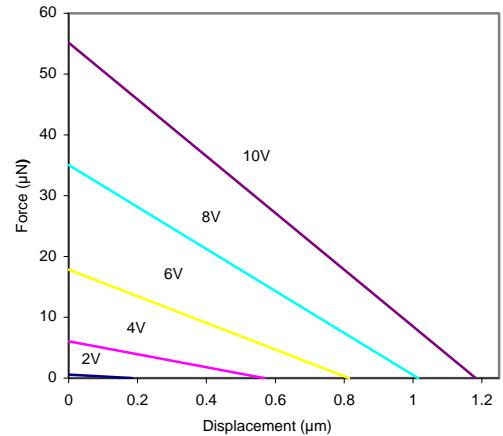


Figure 10: Force-displacement diagram. Calculated by the static blocked and free displacement at different voltage measurements.

To determine the frequency response, the microactuator was electrically stimulated with a sinusoidal waveform (5V DC with 10Vp-p) with a frequency ranging from 1kHz to 10kHz. Amplitudes and angles for displacements are illustrated by

circles in Figures 11 and 12. These measurements exhibit a second-order resonance at 5.7kHz. The phase response exhibits a sharp roll-off at resonance. The noise floor was measured as 2.144 nm (indicated by the dashed line).

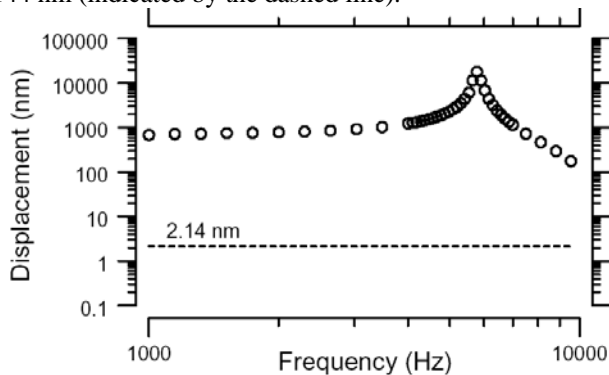


Figure 11: Magnitude of the frequency response of the actuator

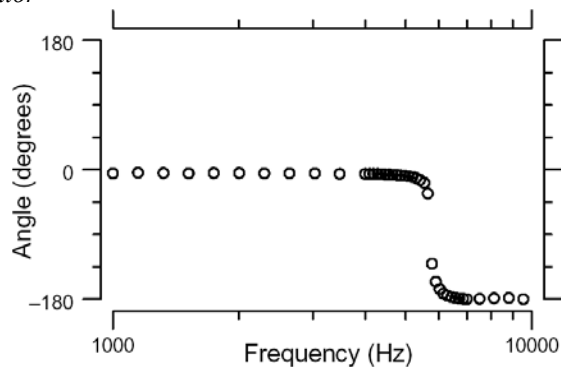


Figure 12: Phase of the frequency response of the actuator

5. EVALUATION

An in-plane piezoelectric micro-actuator was designed and fabricated. Bending of the PZT member (not the end effector) limits the blocked force output. The hybrid actuator demonstrated an amplification ratio estimated to be in excess of 10:1 per cell. Also demonstrated was the ability of the actuator to be fabricated in arrays of micro-actuators, in series, or in parallel, by means of an electrode, or power, bus. New fabrication techniques for PZT were developed, including the patterning of the sol-gel film prior to annealing, and the release of a piezoelectric actuator using XeF_2 . A foundation has now been established for the development of devices which use this actuator, and compliant devices using SU-8, but tests of device fatigue need to be made. After this conservative first design, it is expected to be able to shrink the design to as small as $300 \times 500 \mu\text{m}^2$ with the same performance. Leveraging the arrayability, large stroke, and force of the micro-actuator, novel lateral MEMS RF relays are being developed by the authors.

ACKNOWLEDGEMENT: the authors are grateful to KIMM for the funding of the project, Salil Desai, Stan Jurga, Yong Shi, Raj Sood, Chee Wei Wong and Dr. Yong-bae Jeon. At MTL: Paul Tierney, Dave Terry, Kurt Broderick, Vicky Diadiuk, Dennis Ward, Gwen Donohue, and Bob Bicchieri for their valuable comments and support.

REFERENCES

- [1] C. Niezrecki, D. Brei, S. Balakrishnan, and A. Moskalik, "Piezoelectric Actuation: State of the Art," *Shock and Vib. Digest*, Vol. 33, No. 4, 2001 pp 269-280.
- [2] D. L. Devoe, A. P. Pisano, "Modeling and Optimal Design of Piezoelectric Cantilever Micro-actuators," *Journal of Microelectromechanical Systems*, Vol. 6, No. 3, 1997, pp. 266-270.
- [3] S.G. Kim and M. K. Koo, "Design of a micro-actuator array against the coupled nature of microelectromechanical systems (MEMS) processes", *Annals of the CIRP*, Vol. 49, No. 1, 2000.
- [4] J.L. Steyn, H.Q. Li, D.C. Roberts, K.T. Turner, O. Yaglioglu, Y.-H. Su, M.A. Schmidt, S.M. Spearing, N.W. Hagood, and R. Micak, "Hydraulic Amplification Devices for Microscale Actuation," *Solid-State Sensor, Actuator and Microsystems Workshop*. Hilton Head Island, South Carolina, June 2-6, 2002, pp 50-53.
- [5] Volker Seidemann, Sebastian Bütefisch, and Stephanus Büttgenbach. "Fabrication and Investigation of In-Plane Compliant SU8 Structures for MEMS and Their Application to Micro Valves and Micro Grippers" *Sensors and Actuators A*, Vol. 97-98, 2002, pp. 457-61.
- [6] H. Lorenz, M. Despont, M. Fahrni, N. LaBianca, P. Vettiger, and P. Renaud, "SU-8: a low-cost negative resist for MEMS", *J. Micromech. Microeng* 7(1997) : 121-124.
- [7] Kazunari Maki, Nobuyuki Soyama, Satoru Mori, and Katsumi Ogi, "Evaluation of $\text{Pb}(\text{Zr},\text{Ti})\text{O}_3$ Films Derived from Propylene-Glycol-Based Sol-Gel Solutions," *Japan J. Applied Physics*, Vol. 39 (2000), pp 5421-54.
- [8] D.M.Freeman, A.J.Aranyosi. M.J.Gordon, and S.S.Hong, "Multi-dimensional motion analysis of MEMS using computer microvision," *Digest, Solid-State Sensor and Actuator Workshop 1998*, Hilton Head, SC, pp. 150-155.
- [9] C.Q.Davis, D.M.Freeman, "Statistics of sub-pixel registration algorithms based on spatio-temporal gradients or block-matching," *Optical Engineering*, vol.37, 1998, pp.1290-1298.